ATMOSPHERE

ENSO affects the North Atlantic Oscillation 1 year later

Adam A. Scaife[1,2]*, Nick Dunstone[1], Steven Hardiman[1], Sarah Ineson[1], Chaofan Li[3], Riyu Lu[3], Bo Pang[3], Albert Klein-Tank[4], Doug Smith[1], Annelize Van Niekerk[1,5], James Renwick[6], Ned Williams[2,7]

We demonstrate a 1-year lagged extratropical response to the El Niño–Southern Oscillation (ENSO) in observational analyses and climate models. The response maps onto the Arctic Oscillation and is strongest in the North Atlantic, where it resembles the North Atlantic Oscillation (NAO). Unexpectedly, these 1-year lagged teleconnections are at least as strong as the better-known simultaneous winter connections. However, the 1-year lagged response is opposite in sign to the simultaneous response such that 1 year later, El Niño is followed by a positive NAO, whereas La Niña is followed by a negative NAO. The lagged response may also interfere with simultaneous ENSO teleconnections. We show here that these effects are unlikely to be caused by residual aliasing of ENSO cycles; rather, slowly migrating atmospheric angular momentum anomalies explain both the sign and the timing of the extratropical response. Our results have implications for understanding ENSO teleconnections, explaining observed extratropical climate variability and interpreting seasonal to interannual climate predictions.

The effects of tropical El Niño–Southern Oscillation (ENSO) variability on the extratropical jet streams in the Pacific and Atlantic basins are now well established through the Pacific North American pattern (*1*) and the response of the Arctic Oscillation (AO) and North Atlantic Oscillation (NAO) to ENSO events (*2*–*6*). There is even some evidence that climate change will make Atlantic teleconnections stronger in the future (*7*, *8*).

We know less about longer-term ENSO effects, but the effects of multiyear ENSO events such as double La Niña events have been documented (*9*, *10*). Occasional studies have also argued for lagged effects from single ENSO events, for example, in the stratosphere (*11*) or in the troposphere due to persistent ocean signals and an ocean-atmosphere interaction (*12*, *13*). However, long lagged effects of El Niño and La Niña on the troposphere more than a few months ahead have only been occasionally considered (*14*) because ENSO events tend to decline by boreal spring after their winter peak.

The widely accepted mechanism for teleconnections between ENSO and the extratropics in the same winter (*15*) is through poleward- and eastward-propagating Rossby waves emanating from the Pacific (*16*) or the tropical Atlantic (*17*), and Atlantic effects are strengthened by their interaction with the stratosphere (*5*, *8*, *18*, *19*). However, it has also been shown that ENSO events trigger persistent fluctuations in atmospheric angular momentum (*20*, *21*) and that these propagate slowly poleward (*22*, *23*). Similar persistent and poleward-propagating angular momentum anomalies are maintained and driven by an atmospheric wave–mean flow interaction between transient eddies and the zonal flow in atmospheric models (*23*–*26*), and they even exhibit predictability at interannual lead times, promising a source of long-range predictability of the NAO (*23*).

Given these recent findings, it seems reasonable to ask what implications this interannual mechanism might have for our understanding of ENSO teleconnections in the extratropics. To investigate this question, we used the record of ENSO Nino3.4 sea surface temperatures from HadISST (*27*). Similar results were obtained with other indices such as Nino3, the HadSLP observational dataset of sea-level pressure (*28*), ERA atmospheric reanalysis data (*29*, *30*) from which we calculated atmospheric angular momentum (*23*), and climate model simulations with historic forcings using the HadGEM3 climate model (*31*). We defined ENSO events as those in which Nino3.4 anomalies exceed 0.5 K (Fig. 1) and comprise 41 El Niño and 48 La Niña events. The NAO is the difference in nearest gridpoint pressure at mean sea level (PMSL) between Iceland and the Azores. No detrending was applied, and anomalies are relative to each full record. This does not affect the results because we took differences between El Niño and La Niña events, and these are well distributed throughout the record (Fig. 1).

Lagged teleconnections

The well-known simultaneous winter teleconnection between ENSO and the North Atlantic is shown in Fig. 2A. Differences between composite mean El Niño and La Niña winters over the whole record in Fig. 1 show maximum high-pressure anomalies over Iceland and low-pressure anomalies over the Azores in a pattern resembling the negative phase of the NAO (−1.9 hPa, $P = 0.09$), as found in other studies (*2*). Given the evidence described in the introduction, we also calculated composite mean differences for the winters 1 year after these events. In this case, the sea-level pressure differences in the NAO between El Niño and La Niña (Fig. 2B) are of similar strength but are opposite in sign (+2.3 hPa, $P = 0.05$), with low pressure over Iceland and Greenland and high pressure over the Azores, suggesting that more positive NAO circulation patterns follow El Niño than La Niña in the winter 1 year later. Similar results for the AO are listed in Table 1 and both are statistically significant.

Individual El Niño and La Niña composites also show the reversal in sign 1 year later, but only the differences are large enough to demonstrate statistical significance with current sample sizes. Similarly, the December-January-February (DJF) Southern Annular Mode (SAM), using the Gong and Wang (*32*) index over the more limited period since 1965 due to data fidelity issues (*33*), yields a similar change in sign, with −1.2 hPa during El Niño relative to La Niña and a similar magnitude reversed anomaly of +0.8 hPa in the DJF period 1 year later. However, although the lagged SAM anomaly shows a change of sign similar to that of the Northern Hemisphere, the sample size is too small to demonstrate statistical significance, so hereafter we focus on the NAO and AO.

One obvious possibility for the reversal of sign in the ENSO teleconnection in the following winter is the quasi-oscillatory nature of ENSO itself. To some degree, El Niño tends to be followed by La Niña and La Niña tends to be followed by El Niño, although this latter transition is reported to be less common (*34*). Given the simultaneous winter connection between ENSO phases and the NAO outlined in Table 1, it could in principle be that the reversal of NAO sign simply reflects the reversal of ENSO in the following winter. However, in practice, the composite mean ENSO signal (El Nino minus La Nina) in the following winter (winter 1) is small and is in fact only −0.2 K, ~10% of the +2 K El Niño minus La Niña anomaly present in the concurrent (winter 0) composite shown in Fig. 2A. Given this very small residual anomaly and the fact that the response is of similar strength in both winters, this is not a viable explanation, so we will return to an alternative plausible mechanism later.

The existence of a delayed teleconnection with a lag of 1 year and reversed sign compared with the simultaneous teleconnection implies that the strongest effects of ENSO on the NAO might actually occur when opposite ENSO phases occur in consecutive years. In this case,

[1]Met Office Hadley Centre, Exeter, UK. [2]Department of Mathematics and Statistics, University of Exeter, Exeter, UK. [3]Institute of Atmospheric Physics, Chinese Academy of Sciences, Beijing, China. [4]Delta Climate Center (DCC), Vlissingen, Netherlands. [5]European Centre for Medium-Range Weather Forecasts, Reading, UK. [6]School of Geography, Environment and Earth Sciences, Victoria University of Wellington, Wellington, New Zealand. [7]Max Planck Institute for Meteorology, Hamburg, Germany.
*Corresponding author. Email: adam.scaife@metoffice.gov.uk

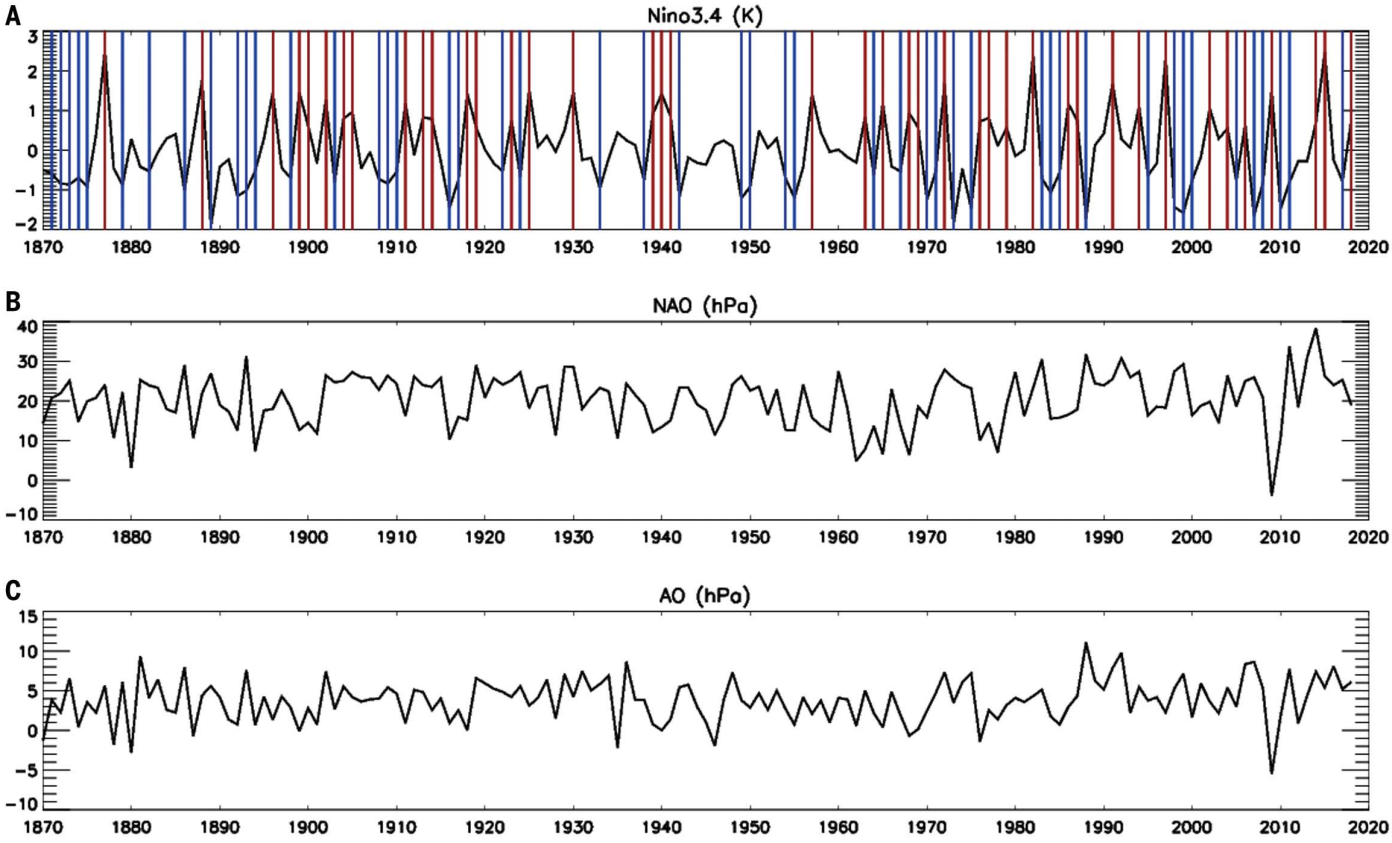

Fig. 1. Series of observed ENSO events, the NAO and the AO. Figure shows the time series of boreal winter ENSO [Nino3.4 (**A**)], the NAO [Azores minus Iceland sea-level pressure (**B**)], and the AO [the difference between area mean sea-level pressure from 45N to 60N and north of 60N (**C**)] used in this study. In the top panel, El Niño and La Niña events are defined as all events in which the magnitude of the anomaly exceeds 0.5 K and are marked by red and blue vertical lines, respectively. All data are for winter (DJF) means.

Fig. 2. Simultaneous and lagged impact of ENSO on the North Atlantic. Shown is the sea-level pressure difference between El Niño and La Niña for simultaneous winters (**A**) and lagged winters 1 year after the ENSO events (**B**) from observational analysis. All data are for winter (DJF) means. Units are hectopascals (hPa), and stippling indicates statistical significance at the 95% level using a one-sided *t* test.

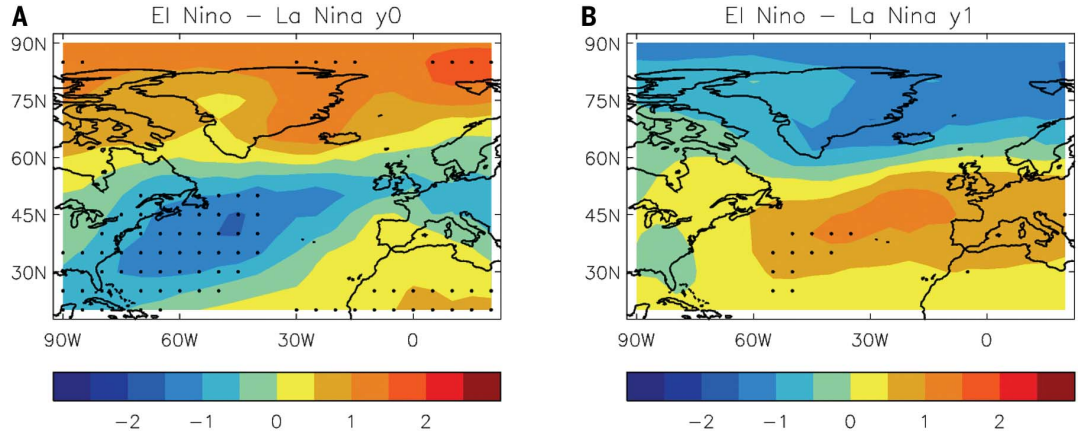

if El Niño is preceded by La Niña, then the well-documented negative winter NAO state from the concurrent El Niño could be amplified by the delayed effect of the preceding La Niña. Similarly, if La Niña is preceded by El Niño, then the positive winter NAO state from the simultaneous La Niña could be amplified by the previous El Niño. This appears to be the case (Table 1), and the delayed teleconnections when ENSO phases are preceded by the opposite phase are of greater amplitude than either the simultaneous or the 1-year lagged responses. Similarly, the reversal of the ENSO teleconnection in the following winter might be expected to lead to little effect in the case of double ENSO events, in which the simultaneous connection to ENSO is negated by the lagged effect of the previous winter. This is also found in the observation record, with no significant NAO anomalies in the second winter of double El Niño (10 cases) or double La Niña (18 cases) events.

A possible mechanism

Previous studies have shown that the sign of the simultaneous connection between ENSO and the NAO can be explained by a combination of the extension of East Pacific anomalies into the Atlantic (*3*) with the effects of increased planetary scale wave forcing of the stratosphere,

weakening the stratospheric polar vortex and leading to a late winter negative NAO (*5*). Given the reversal of the sign of the teleconnection at the 1-year lead time shown above (Fig. 2) and the fact that ENSO declines in the spring, the mechanism for the 1-year lagged effects must be very different.

To explain the year-ahead connection between ENSO and the NAO or AO, we turn to the slow poleward-propagating angular momentum anomalies mentioned above. Figure 3 shows a composite of atmospheric angular momentum integrated over the depth of the atmosphere as a function of latitude and time during and after winter ENSO events. The figure shows El Niño minus La Niña anomalies, but individual El Niño or La Niña cases look similar and have opposite signs.

When they occur, El Niño (La Niña) events generate positive (negative) angular momentum anomalies in the tropical atmospheric circulation near 20 degrees latitude. These anomalies show a high degree of symmetry about the equator that is consistent with their tropical origin. They also reflect the well-known strengthening (weakening) of the subtropical jets (*35*) during El Niño (La Niña) as shown in the early months in Fig. 3. After this and the decline of the ENSO events in the spring, the angular momentum anomalies then persist and migrate slowly poleward due to positive eddy feedback and wave-driven fluxes of angular momentum until the anomaly reaches the source of the eddies in the midlatitudes ~1 year later (*23*).

Inspection of the migrating anomalies in Fig. 3 shows that positive (negative) anomalies reach the midlatitudes by the following winter, suggesting a strengthened (weakened) midlatitude westerly flow and thus positive (negative) NAO and AO 1 year after the El Niño (La Niña) event. This is in agreement with the signs of the anomalies shown in Fig. 2 and Table 1, and suggests that the slow poleward propagation of atmospheric axial angular momentum anomalies may enable lagged and reversed teleconnections from ENSO to the extratropics 1 year after the event.

Reproduction in a climate model

Having demonstrated a year-ahead teleconnection between ENSO and the NAO in observational analyses, an obvious subsequent question is to ask whether the same effect can be reproduced in a climate model. To answer this, we performed the same composite analysis of simultaneous and year-ahead winter composites of sea-level pressure using output from a high-resolution version of the HadGEM3 model with an ~25-km atmospheric grid spacing and a low-resolution version of the same model with an ~100-km atmospheric grid spacing (*31*, *36*). The model simulations use historical forcing and run from 1950 to 2015. There are four members at high resolution and six members at low resolution, resulting in a total of 83 El Niño events and 72 La Niña events in this model-based analysis.

Figure 4 shows the resulting pressure anomaly for ENSO, which is similar to that shown in Fig. 2 for the simultaneous winter and the winter 1 year later for both high- and low-resolution models. As was seen in the observational analysis, the difference between modeled El Niño and La Niña winters resembles the negative phase of the NAO, as expected from the known teleconnection between ENSO and NAO. It also shows an amplitude similar to, though slightly weaker than, the observed composite (*37*, *38*). Furthermore, during the following winter, 1 year after the ENSO event, both high- and low-resolution models also show a clear lagged teleconnection opposite in sign to the simultaneous teleconnection and in reasonable agreement with the pattern and amplitude of the observed teleconnection shown in Fig. 1. The models evidently reproduce a year-ahead Atlantic teleconnection to ENSO. Close inspection suggests that the higher-resolution model produces a slightly stronger teleconnection, but the difference is small, so whether low-resolution models in general are able to reproduce the lagged teleconnection will be an important topic for future research.

Notwithstanding the agreement between the propagating angular momentum anomalies in Fig. 3, which predict both the sign and timing of the year-ahead teleconnection in the model, one might again argue that this could simply be a result of the quasi-oscillatory nature of ENSO and the tendency for La Niña to be followed by El Niño and vice versa. However, just as in the observational case, this effect does not appear to be large enough to explain the modeled year-ahead teleconnection strength: The mean winter Nino3.4 values 1 year after El Niño and La Niña events

Table 1. Magnitude of ENSO teleconnections to the winter AO and NAO. One-year lagged teleconnections (winter 1, right) have similar magnitude to simultaneous connections (winter 0, left, 89 cases for NAO and AO since 1870). Stronger winter teleconnections are found when El Niño (E) is followed by La Niña (L) or L is followed by E (14 cases each, lower rows). Statistical significance values were calculated according to a one-tailed *t* test because the sign of the expected anomaly is known a priori, as explained in the main text.

	Teleconnections (hPa)	
	Winter 0	**Winter 1**
NAO (E minus L)	−1.9 (P = 0.09)	+2.3 (P = 0.05)
AO (E minus L)	−0.80 (P = 0.02)	+0.88 (P = 0.06)
NAO (E followed by L)		+2.6 (P = 0.07)
NAO (L followed by E)		−5.0 (P = 0.003)

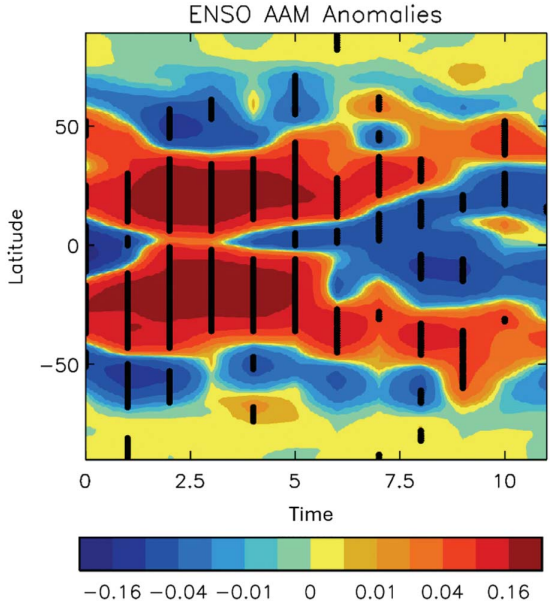

Fig. 3. Migration of ENSO triggered atmospheric angular momentum anomalies into the extratropics. El Niño minus La Niña zonal mean angular momentum anomalies per unit area (10^{10} kg^{-1}) are plotted from the start of events in November to 1 year later from atmospheric reanalyses. The subset of ENSO events in Fig. 1 from 1960 to 2017 were used in this analysis. Note how the positive and negative anomalies originate in the tropics from El Niño and La Niña events and migrate all the way to the midlatitudes 1 year later. Stippling indicates statistical significance at the 95% level using a one-sided *t* test.

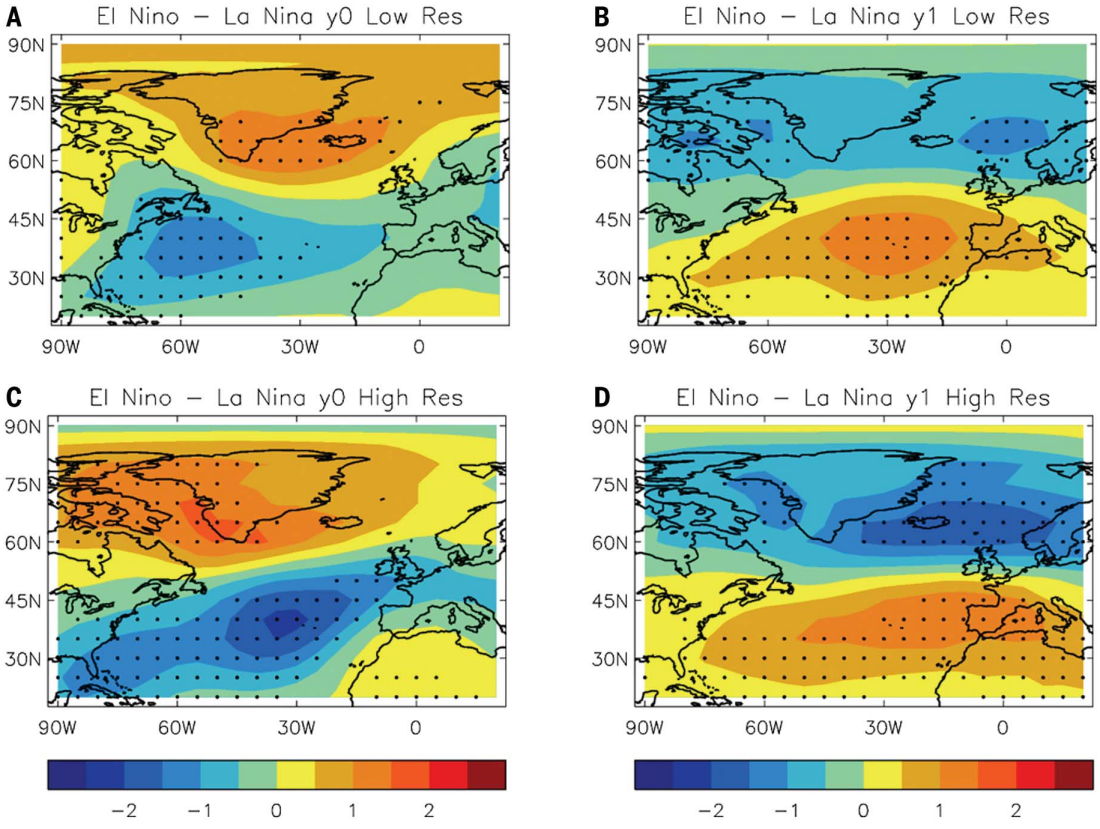

Fig. 4. Modeled simultaneous and lagged impacts of ENSO on the North Atlantic. (**A** to **D**) Sea-level pressure difference between El Niño and La Niña from historical climate model simulations for simultaneous winters [(A) and (C)] and lagged winters 1 year after the ENSO events [(B) and (D)] with low resolution [(A) and (B)] and high resolution [(C) and (D)]. All simulations were performed with the HadGEM3 model. Units are hectopascals (hPa), and stippling indicates statistical significance at the 95% level using a one-sided *t* test.

is again small (−0.26 K) compared with the modeled anomalies of 2.3 K for the simultaneous winter differences between El Niño and La Niña. Given that the teleconnections to the Atlantic in the following winter are again of a magnitude comparable to those of the simultaneous connections, this suggests that, as was the case in the observations, the quasi-oscillatory nature of ENSO is not strong enough to explain the year-ahead teleconnection.

The above arguments are based on the assumption of linearity in the extratropical response. In principle at least, a nonlinear response to ENSO (*17*, *39*) coupled with a few strong events in the second winter could generate a larger response than what is implied by the small mean ENSO anomaly in the second winter. To test this possibility, we need cases in which the second winter contains no ENSO event. The observed events are small in number when we further subset for no second winter ENSO event. However, our model datasets are larger, so we recalculated the lagged NAO composites for modeled ENSO events that had no ENSO reversal event in the next winter. The resulting lagged NAO anomalies (El Niño minus La Niña cases) are 1.7 hPa for winters with no follow-on ENSO event. The 1-year lagged NAO effect is therefore present even when the ENSO event is followed by a neutral ENSO winter. The amplitude of ~2 hPa is also comparable to the observed effect shown in Table 1, and confirms that the lagged effect occurs even in the absence of a subsequent ENSO event.

Conclusions

It is now well established that ENSO events drive winter teleconnections in the extratropical Atlantic sector. The mechanism for these simultaneous effects relies on Rossby wave propagation poleward and eastward from the tropical sources of waves and interaction with the extratropical winter stratosphere. These features can be reproduced, for example, in seasonal forecasts, which show similar predictable wave trains driving predictability of the NAO (*40*).

Here, we argue for a second, delayed teleconnection between ENSO and the extratropical NAO and AO. Despite the extended time lag of 1 year and the complete decay of the ENSO event itself, the strength of this year-ahead (winter 1) ENSO teleconnection is similar in strength to the concurrent (winter 0) teleconnection. The sign of this interannual effect is opposite to the simultaneous teleconnection, and this sign reversal is in agreement with the sign and timing of slow, poleward-propagating zonally averaged angular momentum signals.

A picture now emerges of two mechanisms and two teleconnections between ENSO and the extratropical NAO and AO: In the concurrent winter (DJF0), poleward propagation of Rossby waves drives a negative (positive) AO in response to El Niño (La Niña), whereas 1 year later in winter (DJF1), a prolonged wave mean flow interaction gives a positive (negative) AO in response to the previous El Niño (La Niña). The schematic in Fig. 5 illustrates these two effects and how alternating phases in consecutive winters can amplify the Atlantic response.

There are further implications of these interannual ENSO effects. The interannual teleconnections imply that knowledge of the previous winter ENSO event is important for understanding long-range predictions of the extratropics. For example, after an ENSO event, the probability of the expected NAO sign in the following winter is 10% higher than the probability of the opposite-sign NAO (55 versus 45%), and this result is strengthened when we take into account the expected extreme cases in which El Niño is followed by La Niña or vice versa (as listed in Table 1). In these cases, the probability of the expected sign is double the probability of the opposite sign (68 versus 32%) and is significant at the 95% level. The lagged teleconnections offer a mechanism for the interannual predictability of the NAO (*41*) and the high sensitivity of seasonal and interannual forecasts of the AO or NAO to atmospheric initialization (*42*, *43*). They also imply that understanding the historical midlatitude climate record requires consideration of preceding ENSO events and that there are likely to be effects at other times of year as these signals migrate slowly poleward after winter

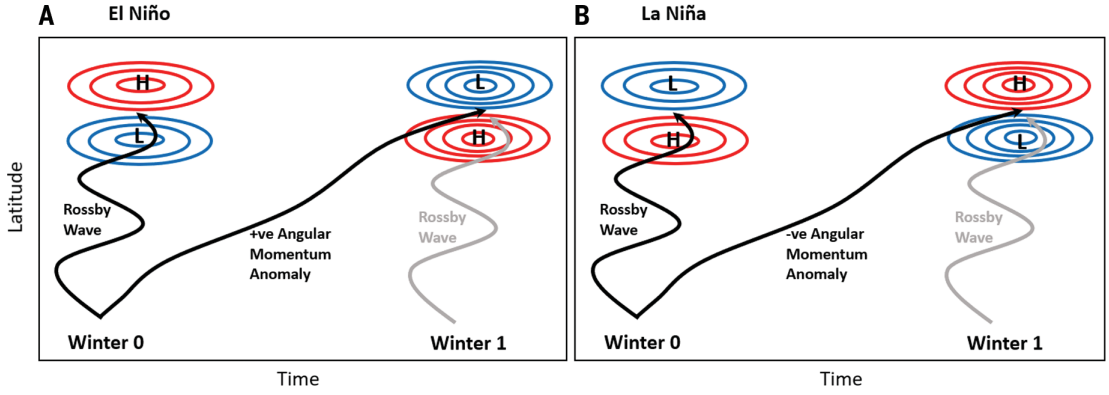

Fig. 5. Mechanism of concurrent and lagged teleconnections between ENSO and the North Atlantic. Both Rossby waves (wavy lines) and slowly propagating zonal mean anomalies (undulating lines) emanate from El Niño events (**A**) and La Niña events (**B**). In the concurrent winter (winter 0), El Niño produces a negative NAO signal (A) and La Niña produces a positive NAO signal (B). One year later (winter 1), slow poleward-propagating angular momentum anomalies create the opposite NAO signals, with positive NAO signals after El Niño and negative NAO signals after La Niña. These signals are amplified if El Niño in winter 0 is followed by La Niña in winter 1 (left) or La Niña in winter 0 is followed by El Niño in winter 1 (right).

ENSO events. Finally, we need a deeper understanding of how well the transient eddy forcing, which provides the driving force behind the poleward-propagating angular momentum anomalies (*23*, *44*), is represented in climate predictions and projections and whether it sufficiently amplifies and persists modeled ENSO teleconnections (*12*, *36*, *45*, *46*), including the lagged teleconnection to the Atlantic shown here.

REFERENCES AND NOTES

1. J. Derome, H. Lin, G. Brunet, *J. Clim.* **18**, 597–609 (2005).
2. S. Brönnimann, *Rev. Geophys.* **45**, 2006RG000199 (2007).
3. Y. Li, N. Lau, *J. Clim.* **25**, 320–342 (2012).
4. A. H. Butler, L. Polvani, C. Deser, *Environ. Res. Lett.* **9**, 024014 (2014).
5. S. Ineson, A. A. Scaife, *Nat. Geosci.* **2**, 32–36 (2009).
6. B. Rodríguez-Fonseca *et al.*, *Atmosphere* **7**, 87 (2016).
7. W. Müller, E. Roeckner, *Clim. Dyn.* **31**, 533–549 (2008).
8. D. R. Fereday, R. Chadwick, J. R. Knight, A. A. Scaife, *Geophys. Res. Lett.* **47**, e2020GL088664 (2020).
9. M. Hoerling, A. Kumar, *Science* **299**, 691–694 (2003).
10. Y. M. Okumura, P. DiNezio, C. Deser, *Geophys. Res. Lett.* **44**, 11,614–11,623 (2017).
11. R. Ren, M. Cai, C. Xiang, G. Wu, *Clim. Dyn.* **38**, 1345–1358 (2012).
12. N. Lau, A. Leetmaa, M. J. Nath, H. Wang, *J. Clim.* **18**, 2922–2942 (2005).
13. H. Su, J. D. Neelin, J. E. Meyerson, *J. Clim.* **18**, 4195–4215 (2005).
14. J. Lin, T. Qian, *Sci. Rep.* **9**, 17543 (2019).
15. J. D. Horel, J. M. Wallace, *Mon. Weather Rev.* **109**, 813–829 (1981).
16. B. J. Hoskins, D. J. Karoly, *J. Atmos. Sci.* **38**, 1179–1196 (1981).
17. T. Toniazzo, A. A. Scaife, *Geophys. Res. Lett.* **33**, 2006GL027881 (2006).
18. E. Manzini, M. A. Giorgetta, M. Esch, L. Kornblueh, E. Roeckner, *J. Clim.* **19**, 3863–3881 (2006).
19. C. Cagnazzo, E. Manzini, *J. Clim.* **22**, 1223–1238 (2009).
20. B. F. Chao, *Geophys. Res. Lett.* **11**, 541–544 (1984).
21. R. S. Gross, S. L. Marcus, T. M. Eubanks, J. O. Dickey, C. L. Keppenne, *Geophys. Res. Lett.* **23**, 3373–3376 (1996).
22. J. O. Dickey, S. L. Marcus, R. Hide, *Nature* **357**, 484–488 (1992).
23. A. A. Scaife *et al.*, *Nat. Geosci.* **15**, 789–793 (2022).
24. I. N. James, J. P. Dodd, *Q. J. R. Meteorol. Soc.* **122**, 1197–1210 (1996).
25. S. Lee, S.-W. Son, K. Grise, S. B. Feldstein, *J. Atmos. Sci.* **64**, 849–868 (2007).
26. G. Chen, P. Zurita-Gotor, *J. Atmos. Sci.* **65**, 2254–2271 (2008).
27. H. A. Titchner, N. A. Rayner, *J. Geophys. Res. Atmos.* **119**, 2864–2889 (2014).
28. R. Allan, T. Ansell, *J. Clim.* **19**, 5816–5842 (2006).
29. S. M. Uppala *et al.*, *Q. J. R. Meteorol. Soc.* **131**, 2961–3012 (2005).
30. D. P. Dee *et al.*, *Q. J. R. Meteorol. Soc.* **137**, 553–597 (2011).
31. M. J. Roberts *et al.*, *Geosci. Model Dev.* **12**, 4999–5028 (2019).
32. D. Gong, S. Wang, *Geophys. Res. Lett.* **26**, 459–462 (1999).
33. G. J. Marshall, R. L. Fogt, J. Turner, K. R. Clem, *Clim. Dyn.* **59**, 3717–3740 (2022).
34. K. Choi, G. A. Vecchi, A. T. Wittenberg, *J. Clim.* **26**, 9462–9476 (2013).
35. R. Seager, N. I. Harnik, Y. Kushnir, W. A. Robinson, J. Miller, *J. Clim.* **16**, 2960–2978 (2003).
36. M. S. Mizielinski *et al.*, *Geosci. Model Dev.* **7**, 1629–1640 (2014).
37. N. Williams, A. A. Scaife, J. Screen, *Geophys. Res. Lett.* **50**, e2022GL101689 (2023).
38. C. I. Garfinkel *et al.*, *J. Clim.* **35**, 8013–8030 (2022).
39. B. Jiménez-Esteve, D. I. V. Domeisen, *Weather Clim. Dyn.* **1**, 225–245 (2020).
40. A. A. Scaife *et al.*, *Q. J. R. Meteorol. Soc.* **143**, 1–11 (2017).
41. N. Dunstone *et al.*, *Nat. Geosci.* **9**, 809–814 (2016).
42. T. N. Stockdale, F. Molteni, L. Ferranti, *Geophys. Res. Lett.* **42**, 1173–1179 (2015).
43. P. J. Athanasiadis *et al.*, *NPJ Clim. Atmos. Sci.* **3**, 20 (2020).
44. S. Feldstein, S. Lee, *J. Atmos. Sci.* **55**, 3077–3086 (1998).
45. I.-S. Kang, J.-S. Kug, M.-J. Lim, D.-H. Choi, *Clim. Dyn.* **37**, 509–519 (2011).
46. S. C. Hardiman *et al.*, *NPJ Clim. Atmos. Sci.* **5**, 57 (2022).
47. Atmospheric angular momenta data for: A. A. Scaife *et al.*, ENSO affects the North Atlantic Oscillation one year later, Zenodo (2024); https://zenodo.org/records/13383912.

ACKNOWLEDGMENTS

We thank B. Wang for pointing out the "lobster pattern" in Lau *et al.*'s 2005 study (*12*). **Funding:** This work was supported by the UK-China Research & Innovation Partnership Fund through the Met Office Climate Science for Service Partnership (CSSP) China as part of the Newton Fund, the UK Public Weather Service Program, and the Met Office Hadley Centre Climate Programme (HCCP) funded by the UK Department for Science, Innovation and Technology (DSIT). **Author contributions:** A.A.S. conceived the study, wrote the first draft, produced all figures, and did the observational analysis. A.V.N. calculated atmospheric angular momentum from observational reanalysis data. J.R. analyzed the southern annular mode. N.W. analyzed climate model data. All authors, including N.D., S.H., S.I., C.L., R.L., B.P., A.K.-T., and D.S., helped write the manuscript and contributed critical analysis of results. **Competing interests:** The authors declare no competing interests. **Data and materials availability:** The HadSLP and HadISST data used in Figs. 1 and 2 are available from https://www.metoffice.gov.uk/hadobs/. The atmospheric angular momentum data used in Fig. 3 are available from Zenodo (*47*). The HadGEM model data from the HighResMIP project used in Fig. 4 are available from https://esgf-ui.ceda.ac.uk/cog/search/cmip6-ceda/.

Submitted 23 August 2023; accepted 28 August 2024
10.1126/science.adk4671